Available online at www.sciencedirect.com
ScienceDirect
Journal of Nuclear Materials 361 (2007) 1–9
journal of nuclear materials
www.elsevier.com/locate/jnucmat

Determination of neutron exposure of AISI 304 stainless steel from a BWR top guide using retrospective dosimetry

L.R. Greenwood, F.A. Garner *, B.M. Oliver, S.M. Bruemmer

Battelle Pacific Northwest Division, P.O. Box 999, Richland, WA 99352, United States

Received 28 July 2006; accepted 24 October 2006

Abstract

Retrospective dosimetry was used to determine the accumulated neutron exposure of AISI 304 stainless steel removed from the top guide of a boiling water reactor located at the Oyster Creek nuclear power station. The material was removed from areas adjacent to cracks that were observed after ~20 years of operation. Using the plant operational history and a variety of measurements of various radioisotopes or non-radioactive transmutation products produced by irradiation, it was possible to determine the integrated neutron fluence experienced by the cracked region and to specify the accumulated displacement dose. Dose estimates on two separate specimens adjacent to the cracks were found to average 1.5 ± 0.2 dpa, possibly reflecting some uncertainty in measurement but more likely suggesting a small gradient in neutron flux-spectra within the section from which the various analysis specimens were cut. This report demonstrates that it is possible to examine defective components lying outside of the core region and where neutron flux-spectra are not well known, and to use the induced transmutation products to determine the neutron exposure with some confidence by using the examined specimen as its own dosimeter.

1. Introduction

Radiation-induced changes in microstructure, dimension, mechanical properties and corrosion resistance are an important field of study required to insure the continued safe and economic operation of nuclear reactors. One important component of such studies is an accurate determination of the radiation environment, especially the integrated neutron fluences.

It is not always possible to measure directly or calculate with confidence the flux-spectra of a given component, especially if it lies well outside the core boundary, near structural or material discontinuities or if the anticipated exposure is low enough that no materials issues are expected and therefore no surveillance dosimetry was employed. In some situations the neutron flux-spectra also vary with time. An example of such a situation can be found in the top guide that lies above the core region of a boiling water reactor. In this region there is two-phase steam-water flowing through the top guide with the steam fraction varying during a reactor campaign. Thus the neutron spectra also change with time.

* Corresponding author. Tel.: +1 509 376 4136; fax: +1 509 376 0418.
E-mail address: frank.garner@pnl.gov (F.A. Garner).

0022-3115/$ - see front matter © 2006 Elsevier B.V. All rights reserved.
doi:10.1016/j.jnucmat.2006.10.016

In such cases a method that can be employed to determine the integrated exposure is that of 'retrospective dosimetry', whereby the irradiated material is examined using a series of measurements of various radioisotopes or non-radioactive transmutation products produced by irradiation [1]. In effect the component of interest becomes its own dosimeter.

The radioisotopes of interest may arise from transmutation of well-defined alloying components or from trace impurities that are not usually included in the material specification. Transmutant helium and hydrogen are also frequently measured in retrospective dosimetry, although the latter gas can accumulate from both transmutant and environmental sources [2,3]. Helium measurements can be used as an independent check on the derived neutron fluences.

In this paper, we examine the application of retrospective dosimetry to a case involving the AISI 304 top guide that lies above the core of a boiling water reactor (BWR) at the Oyster Creek nuclear power plant. Top guides are grid structures that provide lateral support at the tops of the fuel assemblies. As shown in Fig. 1 the top guide has an 'egg-crate' design consisting of interlocking crossbeams that are 9.1 mm thick plates of mill-annealed Type-304 stainless steel. The mill heat composition was Fe–0.06C–18.33Cr–9.36Ni–1.48Mn–0.59Si–0.026P–0.015S.

Irradiation-assisted stress corrosion cracking consistent with behavior observed in other reactor components at higher dose levels was observed in this top guide, although the available estimate of the accumulated neutron fluences was significantly lower ($\leqslant$1 dpa) than ordinarily expected for such cracking. Therefore, it was necessary to obtain a more accurate determination of exposure using retrospective dosimetry in order to confirm that cracking was indeed occurring at such an unexpectedly low exposure level.

The analysis is complicated somewhat by the absence of archive material which can be used to determine the concentration of trace impurity elements that can be activated by radiation. Cobalt and niobium are especially useful for retrospective dosimetry. If sufficient niobium is available, then long-lived ^{93m}Nb from the ^{93}Nb(n, n′) reaction can be measured to estimate the fast neutron exposure. However, other post-irradiation measurement techniques can be used in the absence of archive material to determine the impurity levels.

An additional complication arises from the day-to-day details of power operation which proceeded in campaigns at various power levels separated by variable shut-down periods as shown in Fig. 2, and also by the fact that the material was last irradiated almost six years before examination, allowing for significant decay of some radioisotopes. The reactor operated from December 23, 1969 to September 4, 1996 for a total exposure of 5881.8 EFPD (effective full power days) calculated at a thermal full-power level of 1930 MW.

Fig. 1 shows the configuration of the top guide and the location of the observed cracks. The microstructural examination of these cracks was reported in Ref. [4]. In that report an early estimate of the exposure was presented as ~0.7 dpa. In this paper, we present the results of our measurements yielding a better estimate of the integrated exposure.

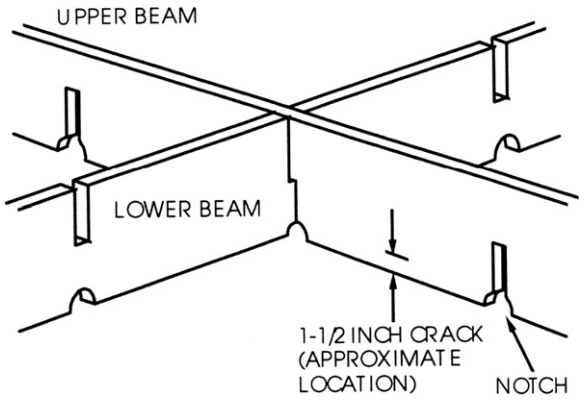

Fig. 1. Egg-crate design of Oyster Creek top guide, showing location of crack with length of ~3.8 cm.

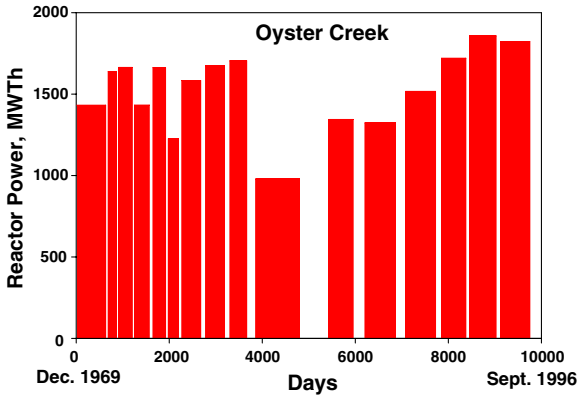

Fig. 2. Power history for the Oyster Creek reactor.

2. Experimental details

The various retrospective dosimetry measurements were performed on a small slice cut from the sample (identified as A3) containing the stress corrosion cracks examined in Ref. [1]. The A3 sample was cut from the crack-tip region and the material for the current analysis was removed from a location adjacent (within ~5 mm) to the crack-tip. The A3 section was subdivided into a number of smaller sections. One of these, the A3A slice, was cut parallel to the A3B slice containing the crack. The A3A slice was further cut, removing four 0.25-mm thick wafers (A3A1 through A3A4) for transmission electron microscopy (TEM) located at an elevation near the end of the crack. TEM disks were punched from these sections and the scrap material was placed in a separate container.

2.1. Sample preparation for gas analysis

Two duplicate samples were received as electropolished TEM disks, originally ~3 mm in diameter and ~0.1 mm thick. Separate specimens were prepared for the helium and hydrogen analyses. The helium analysis specimens were taken from one of the two samples after etching to remove ~0.013 mm of surface material. This etching step was performed to remove material that may have been affected by α-recoil either out of the sample or into the sample from adjacent materials during irradiation. After etching, two approximately one-quarter sections were cut for duplicate helium analyses. The hydrogen analysis specimens were prepared without etching from the second of the two TEM samples. Each duplicate hydrogen specimen represented approximately one half of the second TEM disk.

Each of the analysis specimens was cut using small diagonal wire cutters. Before each use, the cutters were cleaned by wiping several times with a dry 'Kimwipe'. Prior to analysis, each specimen was cleaned in acetone and air-dried. The mass of each specimen was then determined using a calibrated microbalance traceable to the National Institute of Standards and Technology (NIST). The mass uncertainty is estimated to be ±0.002 mg.

2.2. Gas analysis procedure

The helium content of each specimen was determined by isotope-dilution, gas mass spectrometry following vaporization in a resistance-heated graphite crucible in one of the mass spectrometer system's high-temperature vacuum furnaces [5]. The absolute amount of ^{4}He released was measured relative to a known quantity of added ^{3}He 'spike'. Each helium spike was obtained by expanding and partitioning a known quantity of gas through a succession of calibrated volumes [6]. Additionally, the mass spectrometer was calibrated for mass sensitivity during each series of runs by analyzing known mixtures of ^{3}He and ^{4}He.

Hydrogen analyses were also conducted by gas mass spectrometry [7]. The analysis procedure involved dropping the individual specimens, under vacuum, into a small cylindrical ceramic crucible heated to approximately 1200 °C. Prior to analysis, the crucible was pre-heated to approximately 1000 °C under high vacuum for a minimum of 18 h. Before initial vacuum pumping, the sample chamber and crucible volume were subjected to a low-pressure (~200 mTorr or ~27 Pa) argon discharge to aid in desorption of water or hydrated-oxide surface layers that could be dissociated by the hot crucible during analysis, and thus contribute to the measured hydrogen release. During the preheating and subsequent analysis, the sample chamber was maintained at essentially room temperature.

Hydrogen release was measured as a function of time using a quadrupole mass spectrometer connected to the crucible volume. The total hydrogen released was determined from the integral of the hydrogen release curve. Calibration of the system sensitivity was accomplished using a calibrated hydrogen leak source with a stated absolute uncertainty of ±15% (3σ). Calibration measurements were conducted before and after each sample analysis, and showed an overall reproducibility of ~2–3%. Measurements were also conducted on specimens of a standard hydrogen-containing steel (~250 appm hydrogen) maintained in the laboratory. The reproducibility in numerous replicate measurements of this steel is currently averaging about 20% (1σ).

2.3. Gas analysis results

The results of the gas analyses are given in Table 1, and are listed as total atoms of ^{1}H and ^{4}He released, and as gas concentrations in atomic parts per million (10^{-6} atom fraction). Conversion from total gas atoms to gas concentration was based on a calculated value of 1.097×10^{22} atoms/g for the

Table 1
Measured gas concentrations in Oyster Creek top guide materials

Specimen	Material	Mass[a] (mg)	Measured gas release (10^{14} atoms)		Gas concentration (appm)[b]	
			^{4}He	^{1}H	Measured	Average[c]
OYCZ-1	304 SS	2.19	–	85.9	361	363
		2.01	–	79.6	364	±2
OYCZ-2	304 SS	0.485	1.001	–	18.81	18.7
		0.700	1.436	–	18.70	±0.1

[a] Mass of specimen for analysis. Mass uncertainty is ±0.002 mg.
[b] Gas concentration in atomic parts per million (10^{-6} atom fraction) with respect to the total number of atoms in the specimen.
[c] Mean and standard deviation (1σ) of duplicate analyses.

Oyster Creek material. It should be noted, that this conversion value, and the gas concentrations obtained using it, are not very sensitive to small changes in material composition.

The absolute uncertainty (1σ) in the individual helium analysis results, determined from the cumulative uncertainties in the sample mass, the isotope ratio measurement, and the spike size, is estimated to be ~1%. Uncertainty in the hydrogen analyses is estimated at ~20%, and is due largely to the uncertainty in the calibrated hydrogen leak source. An additional uncertainty may also be present from possible hydrogen release from remaining water layers or hydrated metal oxides on the surface of the sample that are subsequently dissociated by the hot crucible.

2.4. Discussion of gas results

The measured helium content in the Oyster Creek sample averaged 18.7 appm. The reproducibility between the duplicate analyses was ~0.5%, which is essentially the same as the inherent analysis system reproducibility, indicating good homogeneity in the helium content. The observed helium is consistent with preliminary calculations based on neutron fluence estimates for the samples. Helium generation arises mainly from both thermal and fast neutron reactions with the steel constituents, especially nickel, but also from lower-energy neutron reactions with the boron impurity in the material.

The measured hydrogen concentration averaged 363 appm, also with a reproducibility of ~0.5%. This level of reproducibility is likely fortuitous given that the variability observed in measurements of our standard hydrogen-containing steel discussed above is closer to ~20%. The observed hydrogen level is consistent with other reactor samples analyzed, and is likely from both (n, p) reactions [8,9] and from hydrogen present in the material prior to irradiation. Given the inherent diffusivity of hydrogen in steel, even at room temperature, it is likely that the observed hydrogen is from trapping sites in the bulk of the material, or trapping sites near the surface.

2.5. Gamma energy analyses

The ^{60}Co activity mainly arises from thermal neutron activation of the impurity cobalt in the steel. ^{60}Co is also produced by two other reactions, namely ^{60}Ni(n, p) ^{60}Co and from the decay of ^{59}Fe to ^{59}Co, which then activates to ^{60}Co. However, calculations indicate that both of these reactions make a negligible (<0.7%) contribution to the ^{60}Co that is produced from the ^{59}Co impurity in the steel. The ^{54}Mn activity is produced by the fast neutron reaction ^{54}Fe(n, p) ^{54}Mn.

The samples for radioactivation measurements were chosen from the scrap produced by punching the TEM disks used for both microscopy and gas analysis. Since the various scrap pieces were mixed after punching of the TEM disks there was not an exact knowledge of the specimen location, introducing some small uncertainty in specimen location. The selected samples were weighed and then gamma-counted using high efficiency intrinsic germanium detectors. The detectors are calibrated relative to NIST and other accepted standards, and control counts are performed daily to ensure continuing energy and efficiency calibrations.

All of the samples showed the presence of ^{60}Co and ^{54}Mn. Due to the long decay time of nearly six years, long gamma counting times were required to accurately measure the ^{54}Mn (312 day) activities. The measured activities and total propagated uncertainties in μCi/mg are listed in Table 2. All of the activities were corrected for decay to the date of

Table 2
Activity measurements (μCi/mg) with 1σ standard deviations[a]

Reaction	Sample 1	Sample 2
Thermal		
$^{62}Ni(n,\gamma)\ ^{63}Ni$	7.45 ± 5%	6.60 ± 5%
$^{54}Fe(n,\gamma)\ ^{55}Fe$	102. ± 5%	105. ± 5%
$^{59}Co(n,\gamma)\ ^{60}Co$	41.6 ± 8%	41.6 ± 8%
Fast		
$^{54}Fe(n,p)\ ^{54}Mn$	1.97 ± 3%	1.64 ± 3%

[a] Values are corrected to September 4, 1996.

the reactor shutdown at the end of cycle 15 on September 4, 1996.

2.5.1. ^{63}Ni measurements

The ^{63}Ni activity is produced by the $^{62}Ni(n,\gamma)$ thermal neutron capture reaction. ^{63}Ni is an excellent thermal neutron monitor since the long half-life of 100 years makes its magnitude relatively independent of the reactor power history.

Sub-samples measuring about 1–2 mg were dissolved in HCl and brought to a known volume in distilled water. Aliquots were taken and spiked with a 2 mg Ni carrier to be used as a yield monitor. After a matrix adjustment, the nickel fraction was purified using an on-column nickel dimethyglyoxime precipitation reaction. Nickel was retained on the column; impurities were eluted with a basic ammonium citrate solution. The nickel was then eluted with 3 M HNO_3. The strip solution was carefully evaporated to near dryness, brought to a known volume with 0.1 M HCl, and split for radiochemical recovery determination by ICP-AES and for ^{63}Ni analysis by liquid scintillation counting. The chemical yields averaged 99%.

Although most of the ^{60}Co activity was chemically separated prior to counting, a minor (<10%) correction for ^{60}Co tailing into the ^{63}Ni region was required using a ^{60}Co standard to determine the beta fraction in the ^{63}Ni energy window (2–70 keV). Calibrations were performed using ^{63}Ni standards obtained from NIST. Sample duplicates showed good repeatability. The decay-corrected ^{63}Ni activities are also listed in Table 2.

2.5.2. ^{55}Fe measurements

The ^{55}Fe activity is produced by the $^{54}Fe(n,\gamma)$ thermal neutron capture reaction. Sub-samples measuring about 1–2 mg were dissolved in HCl and brought to a known volume in distilled water. Iron was stripped from an ion exchange column by passing 6 M HCl, 0.1 M NH_4I through the column. The iodide ion reduced the iron and stripped it from the column. The iron fraction was wet-ashed to eliminate the ammonium salts, and then dissolved in exactly 10.0 ml of 0.5 M HCl.

To mount the samples for X-ray counting for ^{55}Fe, 5.00 ml of the iron solution was measured into a plastic centrifuge tube. NH_4OH was added until $Fe(OH)_3$ precipitated. The $Fe(OH)_3$ was sucked down onto a glass fiber filter. The filter was dried under a heat lamp, then mounted on a cardboard back and covered with thin mylar. The mounts were counted on a low energy photon spectrometer (LEPS) detector for the 6 keV ^{55}Fe X-ray.

The chemical recovery of the iron was measured by ICP-AES analysis of part of the iron product solution. The X-ray counting results for ^{55}Fe were corrected for chemical recovery of the iron, which ranged from 96% to 99%. The ^{55}Fe X-ray standards were prepared in the identical geometry as the samples and the sample masses were very small in order to eliminate the need for absorption corrections. Sample duplicates showed good repeatability. The decay-corrected activities are also listed in Table 2.

2.5.3. Calculation of saturated activation rates

Table 2 lists both the measured activities and the uncertainties corrected to the end of irradiation time for each sample and reaction. Nuclear decay data were taken from Ref. [10]. The activities were converted to saturated activation rates by correcting for the decay during irradiation, atomic weight, elemental abundance, isotopic abundance, gamma self-absorption, neutron self-absorption, and nuclear burnup. These factors are shown in Table 3 and are discussed below. The resultant saturated activation rates are shown in Table 4.

The decay during irradiation was determined using the BCF computer code that integrates the decay of each isotope for each period of reactor operation and downtime shown in Fig. 2. The saturated activities in Table 2 were normalized to a thermal power level of 1930 MW t.

The accuracy of the reactor power history correction factors depends on the half-life of each isotope relative to the details of the irradiation histories. The longer-lived isotopes, such as ^{63}Ni (100 year) truly integrate over the entire irradiation history. Comparison of neutron fluences shown later (Table 6) from the activation data shows that different thermal neutron reactions give reasonably good

Table 3
Correction factors and cross-sections for each reaction

Reaction	At. Wt.	Iso. Abn.	Gabs	History	Cross-sections, barns	
					Thermal	Epi. Cor.
Thermal						
^{62}Ni(n,γ) ^{63}Ni	58.69	0.0363	N/A	0.1696	14.5	16.8
^{54}Fe(n,γ) ^{55}Fe	55.847	0.0585	N/A	1.266	2.3	2.8
^{59}Co(n,γ) ^{60}Co	58.933	1.0	0.993	1.097	37.2	63.1
					>0.1 MeV	>1.0 MeV
Fast						
^{54}Fe(n,p) ^{54}Mn	55.847	0.059	0.990	1.467	0.0380	0.0899

At. Wt. = atomic weight.
Iso. Abn. = isotopic abundance of target (also need elemental abundance in alloy).
Gabs = calculated gamma self-absorption in wires.
History = reactor power history correction for decay.
Thermal = 2200 m/s thermal neutron cross-section.
Epi. Cor. = thermal neutron cross-sections with epithermal corrections, using best fit to the thermal reaction data (ratio = 0.35).

Table 4
Saturated activation rates (atom/atom-second) with 1σ standard deviations[a]

Reaction	Sample 1	Sample 2
Thermal		
^{62}Ni(n,γ) ^{63}Ni	7.60E−11, 5%	7.00E−11, 5%
^{54}Fe(n,γ) ^{55}Fe	1.12E−11, 5%	1.14E−11, 5%
^{59}Co(n,γ) ^{60}Co	2.82E−10, 8%	3.07E−10, 8%
Fast		
^{54}Fe(n,p) ^{54}Mn	1.85E−13, 3%	1.52E−13, 3%

[a] Values are normalized to a power level of 1930 MW t.

agreement confirming the accuracy of the power history corrections.

Estimated gamma self-absorption corrections varied from 1% to 2% for the direct counting of the samples. Neutron self-absorption corrections were not performed since there is no exact knowledge of the location of the individual samples during reactor operation. Nuclear burnup corrections were calculated for the initial and product atoms for each reaction. The highest burnup corrections were about 12% for the ^{59}Co(n,γ) ^{60}Co reaction and less than 5% for the other reactions.

2.6. X-ray fluorescence measurements

The general heat composition for the Type-304 stainless steel used in the top guide was specified in Section 1 but does not specify elements such as cobalt. In order to determine the composition of each specific sample more accurately, sub-samples were analyzed by energy dispersive X-ray fluorescence (EDXRF) techniques at KLM Analytical in Richland, WA.

In this procedure, samples are bombarded with an electron beam and the X-rays are measured with a high-resolution detector. Since the samples were radioactive, X-ray spectra were also taken with the

Table 5
EDXRF analyses of the Oyster Creek top guide material (by KLM analytical)

Element	Sub-sample 1		Sub-sample 2	
	wt%	±	wt%	±
Ti	0.015	0.005	<0.008	
V	0.052	0.005	0.006	0.001
Cr	17.5	1.7	17.7	1.8
Mn[a]	<0.01		0.361	0.037
Fe	71.2	7.1	70.8	7.1
Ni	10.00	1	9.61	0.96
Cu	0.275	0.028	0.344	0.035
Zn	0.138	0.014	0.053	0.005
Ga	<0.002		0.008	0.001
Ge	<0.001		<0.001	
Se	<0.001		<0.003	
Pb	0.068	0.007	0.052	0.005
As	<0.002		<0.001	
Rb	0.078	0.008	0.059	0.006
Sr	0.008	0.001	0.021	0.002
Y	<0.002		0.005	0.001
Zr	0.037	0.004	0.028	0.003
Nb	<0.001		0.017	0.002
Mo	0.257	0.026	0.232	0.023
WDXRF				
Co	0.0789	0.020	0.0715	0.018

[a] The Mn value has a large uncertainty due to interference from ^{55}Fe X-rays.

beam off and this background was subtracted from each EDXRF X-ray spectrum.

NIST 304L stainless steel standards were analyzed at the same time to calibrate and verify the performance of the equipment and inter-element corrections. The results of the X-ray measurements are listed in Table 5. Due to interferences in the EDXRF measurements, the Co content was also measured using the more sensitive WDXRF (wavelength dispersive X-ray fluorescence) technique.

Unfortunately, the EDXRF measurements show that there is insufficient Nb in the sample to confidently measure ^{93m}Nb from the ^{93}Nb(n, n′) reaction and thereby obtain another estimate of the fast fluence.

3. Neutron fluence evaluations

The corrected saturated activities listed in Table 4 are quoted in product atom per target atom per second. These values are equal to the integral over neutron energy of the neutron activation cross-section times the neutron flux spectrum. The thermal neutron fluence can be obtained by dividing the saturated activities by the 2200 m/s thermal neutron cross-section and multiplying by the total irradiation times using cross-section data obtained from the National Nuclear Data Center at Brookhaven National Laboratory (values listed in Table 3) [11].

A better estimate of the thermal neutron fluences can be obtained by correcting for the presence of epithermal neutrons, as is done for the values in Table 6. A simple way to do this is to set each saturated activity equal to the sum of the thermal flux times the thermal cross-section plus an epithermal flux times the resonance integral. This correction is also listed in Table 3 using a ratio of the epithermal to thermal flux of 0.35. This ratio was varied to obtain the best fit to the data.

It should be noted that the thermal neutron fluences are quoted as the 2200 m/s values. The thermal neutron fluence residing below 0.5 eV, typical of what is calculated with computer codes, is a factor of 1.128 times the fluence at 2200 m/s. A further correction to the thermal neutron fluence is required for the operating temperature of the reactor. A typical BWR temperature of 500 °F (260 °C) would require a net correction factor of 1.52 times the 2200 m/s value. In this case, the thermal cross-sections listed in Table 3 would be reduced by the same factor such that the reaction rates for the thermal neutron reactions would remain unchanged.

Table 6
Neutron fluences (n/cm^2 × 10^{21}) with 1σ uncertainties for the top guide samples

Reaction	Sample 1	Sample 2
Thermal[a]		
^{62}Ni (n, γ) ^{63}Ni	2.30, 5%	2.12, 5%
^{54}Fe (n, γ) ^{55}Fe	2.08, 5%	2.12, 5%
^{59}Co (n, γ) ^{60}Co	2.27, 8%	2.47, 8%
Average	2.22	2.19
Std. Dev.	±6%	±8%
Fast >0.1 MeV		
^{54}Fe(n, p) ^{54}Mn	2.47, 10%	2.03, 10%
Fast >1.0 MeV		
^{54}Fe(n, p) ^{54}Mn	1.04, 10%	0.859, 10%

[a] Thermal fluence using 2200 m/s cross-sections with an adjusted epithermal fluence ratio of 0.35 (see text, and Table 3). Thermal group fluences <0.5 eV at reactor operating temperature are about a factor of 1.52 higher than the 2200 m/s value.

The gamma counting data was also used to estimate the fast neutron fluence. In order to accurately determine the fast fluence above 1.0 MeV, or any other energy threshold, it is necessary to know the energy dependence of the neutron flux spectrum. These spectral-averaged activation cross-sections were calculated using the Oyster Creek top guide neutron spectrum from the RAMA calculation, as shown in Fig. 3, and the values are listed in Table 3.

Absolute uncertainties are estimated to be ±10% (1σ), arising mainly from the uncertainty in the calculation of the spectral-averaged cross-sections. Table 6 lists the neutron fluences and estimated uncertainties above 0.1 and 1.0 MeV at each position.

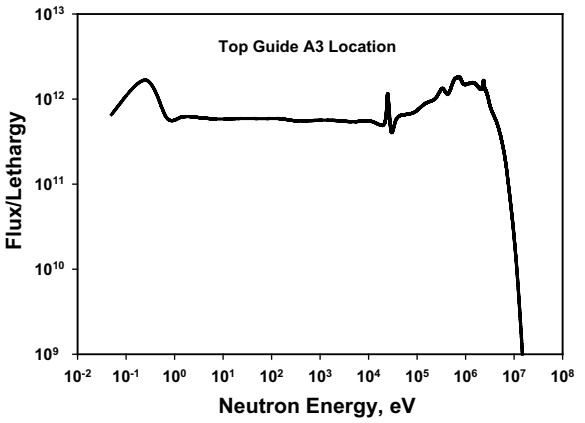

Fig. 3. Neutron flux-spectra from RAMA calculation.

Table 7
Radiation damage parameters for the Oyster Creek top guide samples (boron contributions to the helium are not included since the boron was not measured)

Parameter	Sample 1	Sample 2
dpa	1.64	1.36
Helium, appm		
Fast	0.88	0.72
^{59}Ni	14.8	14.5
Total	15.7	15.2
Hydrogen, appm		
Fast	14.2	11.7
^{59}Ni	2.5	2.4
Total	16.7	14.1

4. Radiation damage calculations

Displacement per atom (dpa) values are calculated by first calculating the ratio of the dpa per 10^{22} fast neutrons >1.0 MeV using the Oyster Creek top guide neutron spectrum and shown in Fig. 3 as input to the SPECTER computer code [12]. This ratio is then multiplied by the fast fluences in Table 6 to determine the dpa, as given in Table 7 for AISI 304 stainless steel.

The gas production is similarly calculated using the SPECTER reaction rates. However, the additional gas from the ^{59}Ni reactions must also be added [13], as also shown in Table 7. The measured helium value for sample 2 was 18.7, only somewhat higher than the calculation at 15.2 appm, although part of the difference could be due to boron in the steel, which is unknown at this point. Perfect agreement can be obtained by assuming a boron content of 3.5 wppm, which is typical for such samples.

The hydrogen was measured for sample 1 to be 363 appm. This is much higher than the transmutation calculation of 16.4 appm; however, this level of hydrogen is typical of many unirradiated materials [14,15] and unirradiated top guide material was not available for comparison.

5. Discussion

All of the measured activities were converted to saturated activation rates by taking into consideration the reactor power history. Thermal and fast neutron fluxes were determined using spectral-averaged neutron cross-sections determined for a typical BWR neutron flux spectrum.

The thermal and fast neutron fluences have been determined via retrospective dosimetry with uncertainties <10% (1σ). The fast ($E > 1$ MeV) fluence varied from 0.86 to 1.04×10^{21} neutrons/cm^2, when measured for two separate specimens, but the thermal fluence (2200 m/s value) varied less, ranging from 2.19 to 2.22×10^{21} neutrons/cm^2. These results imply thermal/fast ($E > 1$ MeV) neutron ratios of 2.1–2.5 for the two separate specimens. Variations of this magnitude are not uncommon due to the somewhat different locations of the two specimens, although this variation is within the range of the uncertainties in the fluence measurements. The thermal-to-fast ratio is also known to vary with distance from the water-cooled surface of the plate [2,3].

Whereas the thermal fluences were determined with several different reactions, the fast fluences could only be determined from the ^{54}Fe(n, p) ^{54}Mn reaction since the long decay time precluded the measurement of ^{58}Co from the ^{58}Ni(n, p) reaction and there is insufficient Nb in the sample to measure ^{93m}Nb from the ^{93}Nb(n, n′) reaction. The thermal neutron fluences from the different reactions are in reasonably good agreement and the absolute accuracy should be close to the standard deviation values quoted in Table 6.

The small variation in dpa levels from 1.64 to 1.36 might be considered to be very good (1.50 ± 0.14) and may also reflect a difference in position from which the two specimens were obtained within the A3A sample volume. The relatively good agreement of predicted and measured helium provides an excellent independent indication that the derived fluence/spectral information is reasonably accurate. Perfect agreement can be obtained by assuming a natural boron content of about 3.5 wppm. Such a boron level is within the range of values usually seen in reactor steels.

A broader study of gas production in BWR reactors shows good agreement between calculations and measurements at a variety of reactor locations [16].

6. Conclusions

It has been shown in this study that reasonably accurate determinations of neutron fluences and accumulated displacement dose can be derived using retrospective dosimetry measurements from reactor components whose nuclear environment is rather difficult to calculate. This approach utilizes transmutation-induced radionuclides or stable atoms produced in the material during irradiation, but this

method requires reasonably accurate knowledge of reactor power history in order to properly incorporate the effect of radioisotope decay during and after power operation.

In the particular case studied in this effort it was shown that cracks developed in a BWR top guide indeed occurred at a relatively low exposure dose on the order of ~1 dpa.

Acknowledgements

This work was sponsored by the Cooperative Irradiation-Assisted Stress Corrosion Cracking Research Program under EPRI project EP-P2291/C1028, and by the US Department of Energy, Materials Science Branch under Contract DE-AC06-76RLO with Battelle Memorial Institute. The specimens were supplied by Emory Hoshi and the hot cell metallographers at G.E. Vallecitos Nuclear Energy Center. The BWR neutron spectra were provided by the BWRVIP-126: BWR Vessel and Internals Project, RAMA Fluence Methodology Software Version 1.0, *EPRI CD 1007823*, 2003.

References

[1] L.R. Greenwood, B.M. Oliver, Retrospective Reactor Dosimetry for Neutron Fluence, Helium, and Boron Measurements, Reactor Dosimetry in the 21st Century, World Scientific, 2002, p. 32.

[2] F.A. Garner, L.R. Greenwood, in: 11th International Conference on Environmental Degradation of Materials in Nuclear Power Systems – Water Reactors, 2003, p. 887.

[3] F.A. Garner, E.P. Simonen, B.M. Oliver, L.R. Greenwood, M.L. Grossbeck, W.G. Wolfer, P.M. Scott, J. Nucl. Mater. 356 (2006) 122.

[4] L.E. Thomas, S.M. Bruemmer, in: 11th International Conference on Environmental Degradation of Materials in Nuclear Power Systems – Water Reactors, Stevenson WA, August 10–14, 2003, p. 1049.

[5] H. Farrar, B.M. Oliver, J. Vac. Sci. Technol. A 4 (1986) 1740.

[6] B.M. Oliver, J.G. Bradley, H. Farrar, Geochim. Cosmochim. Acta 48 (1984) 1759.

[7] B.M. Oliver, F.A. Garner, L.R. Greenwood, J.A. Abrefah, J. Nucl. Mater. 283–287 (2000) 1006.

[8] L.R. Greenwood, F.A. Garner, J. Nucl. Mater. 233–237 (1996) 1530.

[9] F.A. Garner, L.R. Greenwood, B.M. Oliver, in: R.K. Nanstad, M.L. Hamilton, F.A. Garner, A.S. Kumar (Eds.), ASTM STP 1325, Effects of Radiation on Materials: 18th International Symposium, American Society of Testing and Materials, 1999, p. 794.

[10] E. Browne, R. Firestone, V. Shirley, Table of Radioactive Isotopes, Wiley, 1986.

[11] Evaluated Nuclear Data File 533, Version V, National Nuclear Data Center, Brookhaven National Laboratory.

[12] L.R. Greenwood, R.K. Smither, SPECTER: Neutron Damage Calculations for Materials Irradiations, ANL/FPP/TM-197, Argonne National Laboratory, 1985.

[13] L.R. Greenwood, J. Nucl. Mater. 115 (1983) 137.

[14] F.A. Garner, L.R. Greenwood, B.D. Reid, in: Critical Issues Reviews for the Understanding and Evaluation of Irradiation-Assisted Stress Corrosion Cracking, EPRI TR-107159, November 1996.

[15] A.J. Jacobs, in: F.A. Garner, C.H. Henager Jr., N. Igata (Eds.), Influence of Radiation on Material Properties: 13th International Symposium (Part II), ASTM STP 956, 1987, p. 239.

[16] L.R. Greenwood, B.M. Oliver, J. ASTM Int. vol. 3 (2006), JAI13490.